Applied Catalysis B: Environmental 156–157 (2014) 371–377

Contents lists available at ScienceDirect

Applied Catalysis B: Environmental

journal homepage: www.elsevier.com/locate/apcatb

SO_2 poisoning impact on the NH_3-SCR reaction over a commercial Cu-SAPO-34 SCR catalyst

Li Zhang [a], Di Wang [a], Yong Liu [a], Krishna Kamasamudram [b], Junhui Li [b], William Epling [a,*]

[a] University of Houston, Department of Chemical and Biomolecular Engineering, 4800 Calhoun Rd., Houston, TX 77204-4004, United States
[b] Cummins Inc, 1900 McKinley Ave, Columbus, IN 47201, United States

ARTICLE INFO

Article history:
Received 6 January 2014
Received in revised form 13 March 2014
Accepted 17 March 2014
Available online 24 March 2014

Keywords:
Cu-SAPO-34
Selective catalytic reduction
SO_2 poisoning

ABSTRACT

Sulfur poisoning is a durability issue for Cu/SAPO-34 selective catalytic reduction (SCR) catalysts. In this study, the impact of SO_2 on the SCR performance, and the sulfur poisoning mechanism itself, was investigated. SO_2 inhibited SCR activity at low temperature (<300 °C), while at higher temperatures no evident effect was observed. Temperature programmed desorption data show significant SO_2 desorption starting at 300 °C, thus the lack of impact noted at high temperature. Low temperature deactivation is primarily caused by the formation of ammonium sulfate species, with some contribution from competitive adsorption between SO_2 and NO_x, which is considered a key step in the standard SCR reaction, possibly through the formation of metal sulfate species. However, the surface sulfur species decomposed under high temperature thermal treatment in an O_2/N_2 mixture, such that activity was reattained.

1. Introduction

Selective catalytic reduction (SCR) of NO_x by NH_3 is commonly used in diesel engine exhaust after treatment systems. Transition metal exchanged zeolite materials, with the zeolites including ZSM-5, BEA, and SAPO-34 have been studied [1–9]. Recently, chabazite materials have gained significant interest, due to the broad temperature range in which high conversions can be achieved, as well as their improved hydrothermal stability [10–17]. However, Cu/zeolite SCR catalysts are sensitive to sulfur poisoning [3,18,19] and even with ultra-low sulfur fuels, sulfur species can accumulate over time leading to decreased performance.

Diesel oxidation catalysts (DOCs) are typically used in diesel exhaust applications and are located upstream of the SCR catalyst. Therefore, depending on temperature primarily, at least a portion of the SO_2 will be oxidized to SO_3, and with water ever-present, H_2SO_4 formation is also likely. Previous work has suggested that sulfur poisoning by SO_2 differs from that of SO_3. For example, Ramachandran et al. have found that V–ZSM-5 is relatively stable for the SCR reaction in the presence of H_2O and SO_2, but in the presence of SO_3 rapid deactivation was observed. In terms of the mechanism, the authors concluded that ammonium bisulfate formed when both NH_3 and SO_3 were present [19]. Cheng et al. compared deactivation of a Cu/BEA catalyst by SO_2 and SO_3 and found that SO_3 was more significant than SO_2, and the authors proposed that $CuSO_4$ formed upon SO_3 exposure, resulting in deactivation [18]. Their analysis also showed that even after the sulfate formed, the Cu remained in a highly dispersed state, at its initial ion-exchange locations. Jiang et al. [20] studied the poisoning effects of SO_2 over a Fe-Mn/TiO_2 catalyst, and concluded that SO_2 inhibition was due to surface sulfate formed, which in turn affected NO adsorption. Xu et al. [12] investigated a Ce/TiO_2 SCR catalyst and proposed that the SO_2 could react with the catalyst to form thermally stable $Ce(SO_4)_2$ and $Ce_2(SO_4)_3$, which in turn affected redox cycling between Ce(IV) and Ce(III) and inhibited nitrate formation.

Overall, based on the literature, different sulfur poisoning mechanisms of NH_3-SCR catalysts have been proposed. And thus far, the SO_2 deactivation mechanism of Cu/SAPO-34 has not been clearly explained. In the present study, the impact of SO_2 exposure on the SCR performance of a commercial Cu-SAPO-34 sample was characterized. The standard SCR reaction was chosen to examine the impact, with the assumption that the apparent ever-decreasing exhaust temperatures will put more emphasis on the standard SCR reaction over the fast and NO_2-SCR reactions.

2. Experimental methods

The Cu-SAPO-34 catalyst was supplied by Cummins Inc. The Cu-SAPO-34 catalyst sample had a Si/(Al + P) ratio of 0.2. The Cu loading was 0.95 wt.%, as detailed previously [11]. Also, this commercial

* Corresponding author. Tel.: +1 713 743 4234.
E-mail address: wsepling@uh.edu (W. Epling).

http://dx.doi.org/10.1016/j.apcatb.2014.03.030
0926-3373/

Table 1
Gas phase composition of different adsorption phase during TPD experiments.

Experiment	Adsorption phase (balance N_2)
SO_2-TPD	200 ppm SO_2 + 10% O_2
NH_3-TPD	500 ppm NH_3
SO_2 + NH_3-TPD	500 ppm NH_3 + 200 ppm SO_2 + 10% O_2
NO_x-TPD	500 ppm NO + 10% O_2
SO_2 + NO_x-TPD	200 ppm SO_2 + 500 ppm NO + 10% O_2

catalyst contains ceria as an additive, on the order of 2 wt.%. For SCR activity tests, a monolithic-supported sample was used, 1.4″ long and 0.8″ in diameter, which was placed in a quartz tube reactor placed inside a Lindberg temperature-controlled furnace. Before testing, the catalyst was pretreated at 550 °C for 4 h in 10% O_2/N_2. For the reactor experiments, all gases except balance N_2 were supplied by Praxair and were metered by MKS mass flow controllers. Balance N_2 was produced by a N_2 generator manufactured by On-Site. The effluent gas concentrations were measured using a MultiGas 2030 FTIR analyzer. For SCR activity tests, the simulated exhaust gas contained 500 ppm NO, 500 ppm NH_3, and 10% O_2, with a balance of N_2. The total flow rate was 5 L/min, and the corresponding gas hourly space velocity (GHSV) was 28,000 h^{-1}. For SO_2 oxidation, the reaction gas mixture consisted of 200 ppm SO_2, 10% O_2 and a N_2 balance.

To evaluate the performance of the sample with some or all sulfur removed (deSO_x), the S-laden samples were exposed to 10% O_2/N_2 and temperature programmed experiments were carried with a heating rate of 5 °C/min at a flow rate of 5 L/min. The samples were heated to different temperatures and left at those for 12 h.

Temperature-programmed desorption (TPD) experiments were carried out after the catalyst was exposed to SO_2, NH_3, SO_2 + NH_3, NO_x, or SO_2 + NO_x, using the same reactor described above. Typically, the sample was pretreated in 5 L/min of 10% O_2/N_2, while heating from room temperature to 600 °C with a heating rate of 25 °C/min, and was held at 600 °C for 0.5 h and then cooled back to room temperature in 10% O_2/N_2. For the TPD experiments, the adsorption phase was run at 150 °C and with a total flow rate of 5 L/min. This was followed by a purge phase in N_2 for 1 h, and then the temperature was increased from 150 to 735 °C at a rate of 10 °C/min. The gas compositions of each adsorption phase for the different experiments are listed in Table 1. Note, for SO_2 adsorption/desorption experiments, a sulfur mole balance was obtained, within 5% error.

Surface species formed during catalyst exposure to SO_2, NO_x and NH_3 were characterized with in-situ Diffuse Reflectance Infrared Fourier Transform Spectroscopy (DRIFTS). A Nicolet 6700 FT-IR spectrometer equipped with a Harrick Scientific Praying Mantis DRIFTS cell and a mercury-cadmium-telluride (MCT) detector was used. The powder sample was scraped from the monolith sample and was pressed into a 60 mg pellet of 6.5 mm diameter and placed in the sample cup with a porous screen at the bottom surface, allowing the gas to pass through the catalyst from top to bottom. A feed gas mixture, controlled using MKS mass flow controllers, was supplied at a flow rate of 50 mL/min. The samples were first treated in a flow of 10% O_2/He at 500 °C for 0.5 h and then cooled to room temperature. At the temperatures used for analysis, a background spectrum was recorded in flowing He, and it was subtracted from the sample spectrum obtained at the same temperature. The DRIFTS spectra were collected from 4000 to 650 cm^{-1}, accumulating 100 scans at a 4 cm^{-1} resolution. Nicolet OMNIC software was used to convert the absorbance data into Kubelka-Munk (KM) format. The experimental details for the DRIFTS experiments are described below.

The interactions between SO_2 and the surface of the Cu-SAPO-34 catalyst were studied by collecting DRIFTS spectra during exposure to 200 ppm SO_2 and 10% O_2 at 150 °C, with He as the carrier gas. In investigating the interactions between NH_3 and SO_2 adsorbed on the surface of catalyst, the sample was exposed to 500 ppm NH_3 and 500 NH_3 + 200 ppm SO_2, in the presence of 10% O_2, at 150 °C.

The interactions between SO_2 and NO_x on the surface of the catalyst were also investigated. First, DRIFTS spectra were obtained during catalyst exposure to 500 ppm NO + 10% O_2 and then exposing the sample to 200 ppm SO_2 at 150 °C. Second, the effects of SO_2 on NO_x adsorption were also investigated by exposing the sample to 200 ppm SO_2 + 10% O_2 at 150 °C for 60 min, followed by purging in He for 30 min, and then exposing the sample to 500 ppm NO for 60 min. In the third experiment, DRIFTS spectra were obtained while the sample was exposed to 500 ppm NO or 500 ppm NO + 200 ppm SO_2, in the presence of 10% O_2, at 150 °C.

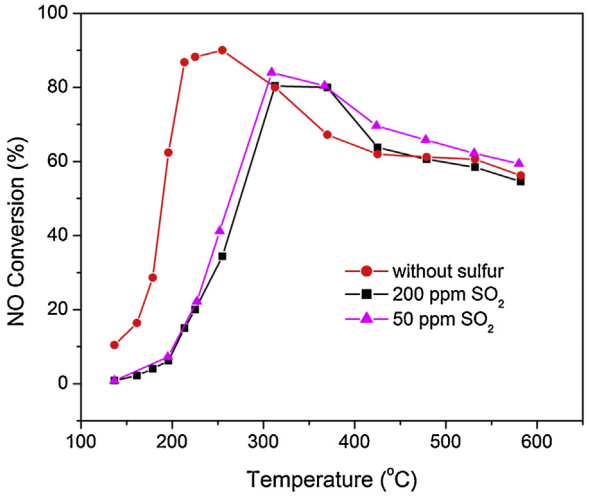

Fig. 1. SCR reaction activity in the absence and presence of SO_2. Reaction conditions: 500 ppm NH_3, 500 ppm NO, 0, 50 or 200 ppm SO_2, 10% O_2 and a balance of N_2, total flow rate 5 L/min, SV = 28,000 h^{-1}.

3. Results and discussion

3.1. SO_2 exposure impact on NH_3-SCR

The standard SCR reaction activity was evaluated over the monolith-supported Cu-SAPO-34 catalyst from 130 to 580 °C, and the NO conversion results in the absence and presence of SO_2 as a function of temperature are shown in Fig. 1. Under the conditions tested, appreciable NH_3-SCR activity was observed in the absence of SO_2 between 130 and 580 °C. About 90% NO conversion was achieved at 200 °C. With increasing temperature, the conversion decreased because of competitive NH_3 oxidation at high temperatures, as evidenced by 100% NH_3 conversion at these temperatures. In addition, very little N_2O (<5 ppm) was detected during these tests, indicating a high selectivity of NO to N_2 was achieved.

The effect of SO_2 on the SCR activity is also illustrated in Fig. 1. Low temperature catalytic activity (130–300 °C) significantly decreased with the addition of 50 ppm SO_2. For example, the NO conversion dropped from 90% to 15% at 200 °C. On the other hand, at temperatures above 300 °C, there is a slight improvement or no impact observed. When 200 ppm SO_2 was added to the system instead of 50 ppm, the poisoning effects on NO conversion were similar, indicating that different concentrations do not lead to different poisoning mechanisms. These inlet SO_2 concentration values are admittedly higher than those found in vehicle exhaust, however, the higher concentrations were used to achieve steady-state conditions in a timely manner. Furthermore, the lack of difference

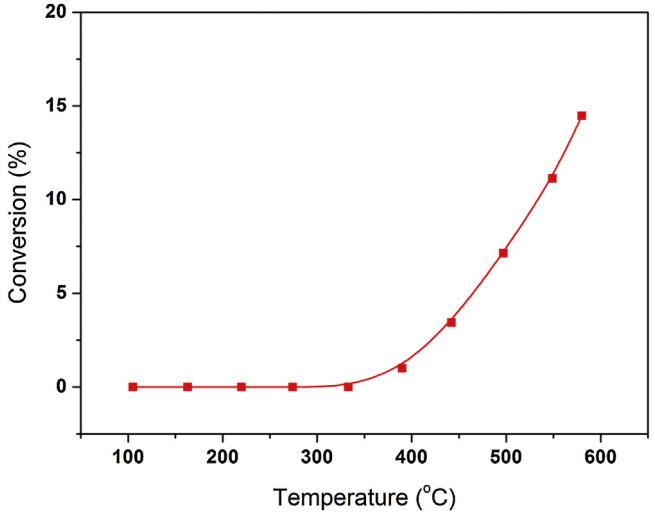

Fig. 2. SO_2 oxidation conversion as a function of temperature. Reaction conditions: 200 ppm SO_2, 10% O_2 and a balance of N_2, total flow rate 5 L/min.

between 50 and 200 ppm SO_2 effects suggests that the chemistry with lower concentrations would remain the same.

3.2. SO_2 oxidation

SO_2 exposure only affected the SCR performance at low temperature. It has been reported that both SO_2 and SO_3 poisoned a Cu-zeolite catalyst and the impact of SO_3 on the SCR reaction [3] differs from that of SO_2, and is indeed more severe. In order to determine whether SO_2 oxidation to SO_3 could occur over the Cu-SAPO-34 sample, and thus lead to a convoluted interpretation of the individual S species effects, SO_2 oxidation activity was evaluated. SO_2 oxidation conversion as a function of temperature is shown in Fig. 2. Interestingly, no SO_3 was detected at temperatures below 300 °C, which is the temperature range that the SO_2 poisoning effect was observed. SO_2 conversion was observed around 400 °C, and increased with increasing temperature, reaching a maximum of only 15% at 580 °C under the conditions of this test. Therefore, the low temperature deactivation observed was not caused by the formation of SO_3. Furthermore, since SO_3 could be formed at higher temperatures during the SCR activity test described above, and no inhibition was observed, it appears that the Cu-SAPO34 catalyst tested is resistant to SO_2 and SO_3 poisoning when operating at high temperatures.

3.3. DRIFTS characterization of $SO_2 + O_2$ adsorption

As discussed above, SO_2 exposure primarily affected SCR reaction activity at low temperatures. The interactions between SO_2 and the surface of the Cu-SAPO-34 catalyst were studied using in-situ DRIFTS in order to better understand this impact. DRIFTS spectra obtained during adsorption of SO_2, in the presence of gas phase O_2, are shown in Fig. 3. During the exposure, several bands in the 1200–1800 cm^{-1} range were detected. The larger feature at 1612 cm^{-1} was assigned to H–O–H vibrations caused by SO_2 interacting with OH groups [12]. Several smaller features at 1434, 1320, 1304, 1287 and 1226 cm^{-1} were observed and these peaks are attributed to the formation of surface SO_2 groups and sulfate species associated with different adsorption sites (e.g. Cu or Ce sites) [12,21,22]. Here, we need to emphasize that since CeO_2 is a part of the catalyst formulation, SO_2 adsorption on CeO_2 is also possible. Features at 3675, 3650, 3558, and 3500 cm^{-1} were also detected during SO_2 exposure. The three positive peaks at 3675,

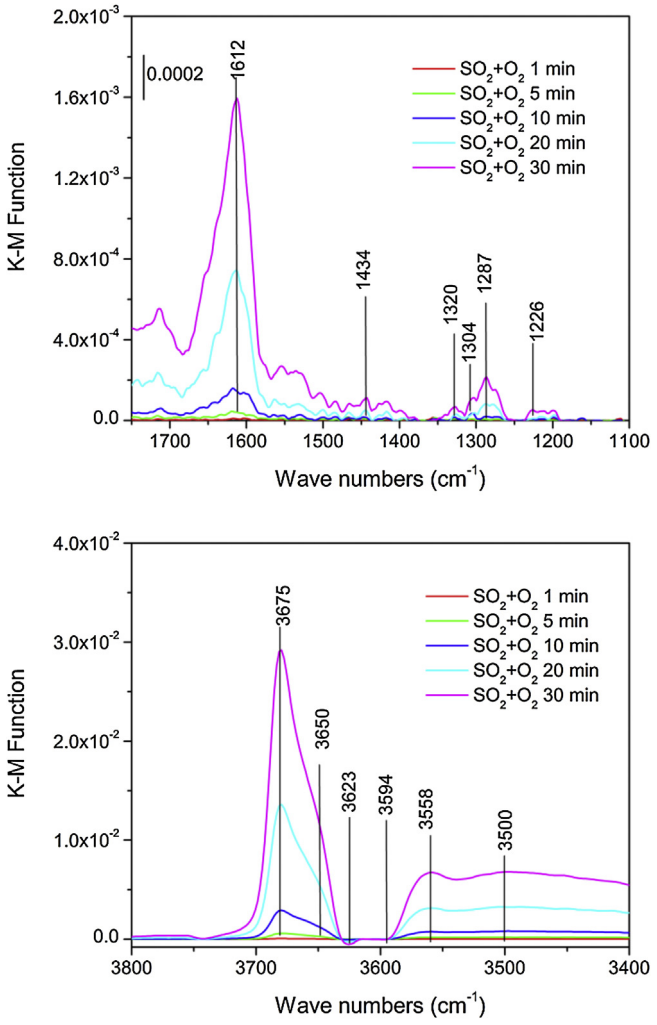

Fig. 3. DRIFTS spectra of adsorbed $SO_2 + O_2$ at 150 °C. Experiment conditions: 150 °C exposure to 200 ppm SO_2, 10% O_2 and a balance of He, total flow rate 50 mL/min.

3650 (shoulder) and 3558 cm^{-1} are assigned to perturbed P–OH, and perturbed OH groups associated with the extra-framework Al and Cu, respectively [19,23,24]. The appearance of a broad band at 3500 cm^{-1} might be due to hydrogen-bonded OH [25]. In addition, two small negative peaks appeared at 3623 and 3594 cm^{-1}, caused by the consumption of Si(OH)Al groups [9,19], associated with Bronsted acid sites, by SO_2. Indeed, previous work has shown that –OH groups participate in the adsorption of SO_2 [26,27]. Marcu et al. proposed that SO_2 molecules could adsorb via hydrogen bonding to surface hydroxyl groups on the zeolite to form hydrogen sulfite OH-OSO or OH-OSO-HO [25]. From these DRIFTS results, it appears that SO_2 reacted with the Cu and/or CeO_2 sites as well as the surface hydroxyl groups.

3.4. Characterization of the interaction between SO_2 and NH_3

NH_3 adsorption is a key step in the SCR reaction, so in order to determine how SO_2 might impact this function, and with the above results suggesting at the least the Bronsted acid sites could be affected, DRIFTS was used to characterize the surface during exposure to NH_3 and co-exposure to $NH_3 + SO_2$. As shown in Fig. 4, NH_3 adsorption produces a significant feature at 1460 cm^{-1} and three weaker ones at 1617, 1280 and 1214 cm^{-1}. The first is assigned to NH_4^+ vibrations, via NH_3 adsorbed on Brønsted acid sites, Si-OH, P-OH or bridging OH sites, and the 1617, 1280 and 1214 cm^{-1} features

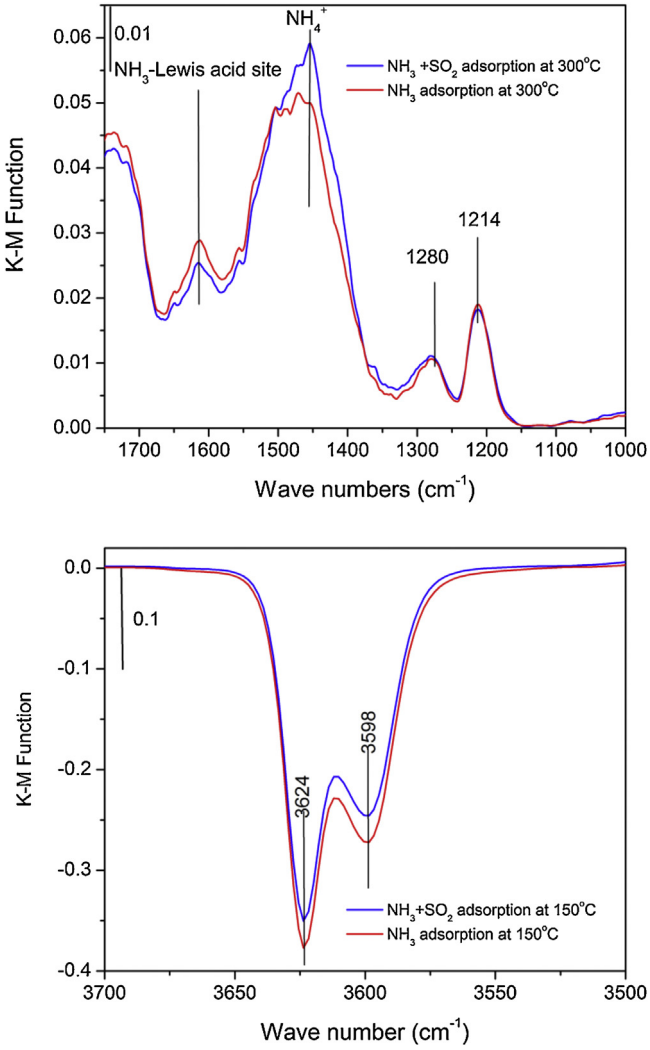

Fig. 4. DRIFTS spectra obtained after a 60 min exposure to NH_3 and $NH_3 + SO_2$ at 150 °C. Experiment conditions: 500 ppm NH_3, 10% O_2 + 200 ppm SO_2 (if added) in a He balance.

to molecularly adsorbed NH_3 bound to Lewis acid sites [11,19,28]. The 1617 cm^{-1} is assigned to Lewis acid sites associated with the exchanged Cu, and the 1280 and 1214 cm^{-1} peaks correspond to Lewis acid sites on transition alumina or on nonframework aluminas on zeolites [28]. In the OH stretching region, negative bands at 3624, and 3598 cm^{-1} were observed, and assigned to bridging OH sites (Al-OH-Si) [11,29]. A fresh catalyst was then exposed to both NH_3 and SO_2. In comparing the band intensities after a 60 minute exposure to both species, to the band intensities during only NH_3 exposure, the features corresponding to NH_3 on the Cu-related Lewis acid sites (1617 cm^{-1}) and OH bridging sites slightly decreased. This indicates a reduction in the amounts of NH_3 on the Brønsted acid and Lewis acid sites. However, the band intensity for the NH_4^+ vibration increased. It did not change in step with the Brønsted acid site feature corresponding to the OH bridging bond, and as will be discussed further below, is due to the formation of new NH_4^+ species. These data show that SO_2 does affect NH_3 adsorption, and might form some new sulfur related NH_4^+ species based on the NH_4^+ feature intensity increase. Note, it is difficult to clearly observe sulfur features during SO_2 co-adsorption with NH_3, due to the weaker intensities of the surface sulfur species IR features (as shown in Fig. 3) compared with the species formed during NH_3 adsorption that result in features in the same range.

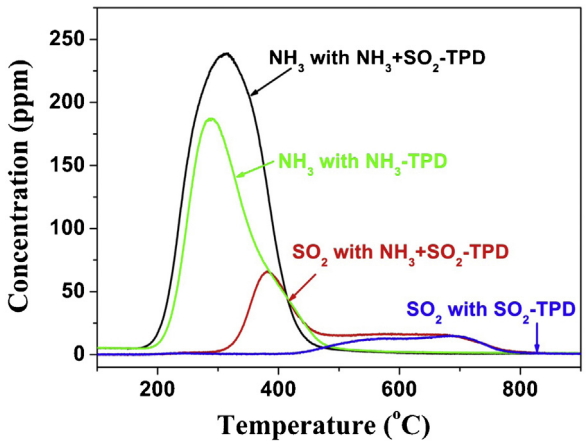

Fig. 5. TPD results after exposure to $SO_2 + NH_3$, NH_3 or SO_2. Experimental conditions: 500 ppm NH_3 (if added), 200 ppm SO_2 (if added), 10% O_2 and a balance of N_2 at 150 °C, purged by N_2, then TPD with a heating rate of 10 °C/min in N_2.

3.5. $SO_2 + O_2$-TPD, NH_3-TPD and $NH_3 + SO_2$-TPD

Temperature programmed desorption (TPD) experiments were performed after the catalyst was exposed to SO_2 and O_2 to characterize SO_2 adsorption/desorption features while at the same time outlet SO_2 and SO_3 gas-phase concentrations were measured. As shown in Fig. 5, after SO_2 adsorption (with 10% O_2 present), SO_2 desorbed from the surface during the TPD between 450 and 750 °C, with two apparent desorption peaks evident, at around 550 °C and 680 °C, which are believed to originate from different adsorption sites. The lower temperature peak is assigned to SO_2 chemisorbed on the catalyst surface as sulfate species, as observed in the DRIFTS spectra (shown in Fig. 3). And the higher temperature peak is likely due to decomposition of $CuSO_4$ or $Ce_x(SO_4)_y$ species that formed, as these typically decompose to SO_2 at a relatively high temperature [30,31], and is consistent with previous observations of metal sulfate poisoning during SO_2 exposure [3,12,18,22]. For example, previous work has shown Cu sulfate species, for a Cu/zeolite catalyst, decompose with SO_2 desorption at temperatures above 500 °C [3], while TPD of SO_2 results with a Ce material shows that Ce related sulfate species decompose at an even higher temperature (~700 °C) [12].

For comparison, TPD experiments were run after the catalyst was exposed to both NH_3 and SO_2. As shown in Fig. 5, with the catalyst just exposed to SO_2, desorption peaks were observed at temperatures higher than 450 °C. However, with exposure to both NH_3 and SO_2, another peak was observed at about 400 °C, with the onset of desorption noted at ~300 °C. In the same figure, NH_3 profiles during the TPD in the absence or presence of SO_2 clearly show that a significantly larger amount of NH_3 was released when the catalyst was also exposed to SO_2 during the adsorption process. Thus, this extra SO_2 feature and larger amount of NH_3 adsorbed can again be associated with the enhancement in the NH_4^+ band observed in the DRIFTS spectrum detailed previously. These data taken together suggest that some surface ammonium-sulfate or ammonium-bisulfate species were formed and decomposed, releasing SO_2 at lower temperature. Indeed, the ratio of this increased amount of NH_3 to the amount of the additional SO_2 that was released at 400 °C is 2:1. This coincides with the typical $(NH_4)_2SO_4$ decomposition reaction that involves the initial decomposition to NH_3 and NH_4HSO_4 at around 300 °C and the surface NH_4HSO_4 species continue to decompose to NH_3 and SO_2 at

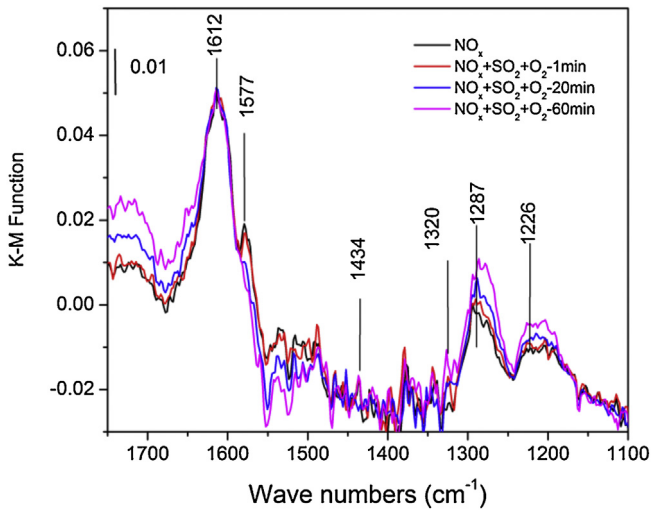

Fig. 6. DRIFTS spectra taken during exposure to SO_2 after exposure to NO + O_2 at 150 °C. Experimental conditions: 500 ppm NO, 10% O_2 in a balance of He, then followed by 200 ppm SO_2, balance He.

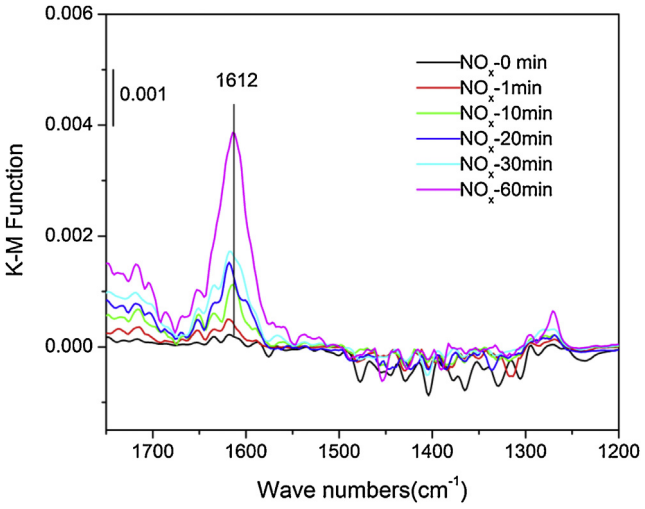

Fig. 7. DRIFTS spectra taken during exposure to NO + O_2 after exposure to SO_2 at 150 °C. Experimental conditions: 200 ppm SO_2 in a balance of He followed by purging and then 500 ppm NO, 10% O_2 in a balance of He, total flow rate 50 mL/min.

higher temperature. Therefore the overall released NH_3 and SO_2 is in a 2:1 ratio.

$$(NH_4)_2SO_{4(S)} \leftrightarrow NH_4HSO_{4(S)} + NH_{3(g)} \quad (1)$$

$$NH_4HSO_{4(s)} \leftrightarrow NH_{3(g)} + SO_{2(g)} + 1/2O_{2(g)} + H_2O_{(g)} \quad (2)$$

3.6. Interaction between SO_2 and pre-adsorbed NO_x

The above results show that SO_2 affected NH_3 adsorption and itself adsorbed to the Cu-SAPO-34 catalyst, with co-adsorption leading to ammonium sulfate formation. The interactions between SO_2 and NO_x were also investigated by comparing the DRIFTS spectra taken during catalyst exposure to NO + O_2 and then exposing the sample to SO_2 after a NO + O_2 exposure. As shown in Fig. 6, bands at 1612 and 1577 cm^{-1} were immediately observed with exposure to NO + O_2. Based on literature studies, these two peaks are tentatively assigned to adsorbed bidentate (1577 cm^{-1}) and bridging (1608 cm^{-1}) nitrate species [28,32,33]. It is also worth noting that the band at 1577 cm^{-1} was not observed during NO + O_2 adsorption on H-SAPO-34 (results shown in Figure S.1 in the supporting information material), and therefore is considered to be a unique feature for bidentate nitrate species formed on Cu sites. When the sample was exposed to SO_2 after it was exposed to NO + O_2, the feature at 1577 cm^{-1}, assigned to the nitrates formed on Cu sites, disappeared with time, whereas features at 1320, 1287 and 1226 cm^{-1} due to the SO_2 adsorbed species increased. The bridging nitrate feature overlaps with a sulfur-related feature, however, in comparing Figs. 3 and 6, it is apparent that these two species result in very different IR signal intensities. Thus, this feature in Fig. 6 is assigned as the nitrate still. These data demonstrate that SO_2 affected NO_x adsorption, specifically the nitrate species formed on the Cu sites.

3.7. Interaction between NO_x and pre-adsorbed SO_2

The interaction between NO_x and pre-adsorbed SO_2 was then investigated by exposing the sample to SO_2 and O_2 first, followed by a He purge, and then exposure to NO + O_2. The DRIFTS results during the NO_x exposure are shown in Fig. 7. With NO_x exposure, a weak peak appeared at 1612 cm^{-1}, assigned to the bridging nitrate species. No bidentate nitrate species feature (1577 cm^{-1}) was apparent.

In addition, the intensity of the NO_x adsorption peak in Fig. 7 is less than that in Fig. 6, demonstrating that less NO_x adsorbed when the sample was first exposed to SO_2 + O_2. Previous research has demonstrated that the bidentate species formed are key intermediates for the low temperature SCR performance of Cu-SAPO-34 [11], and thus SO_2 impacting the formation of this intermediate could also lead to the decreased performance observed at low temperature (Fig. 1).

3.8. Co-adsorption of NO_x and SO_2

In comparison, the same catalyst was subsequently exposed to both NO and SO_2, with O_2. As shown in Fig. 8, the adsorbed bidentate nitrates (1577 cm^{-1}) during NO_x adsorption were not observed during the co-adsorption of SO_2 and NO_x. The bridging (1612 cm^{-1}) nitrate species [28,32,33] feature did appear. It is also worth noting that the band intensity was less than the band's intensity during just NO_x adsorption. These data again prove that SO_2 competes with NO_x for surface adsorption sites, resulting in less NO_x adsorption.

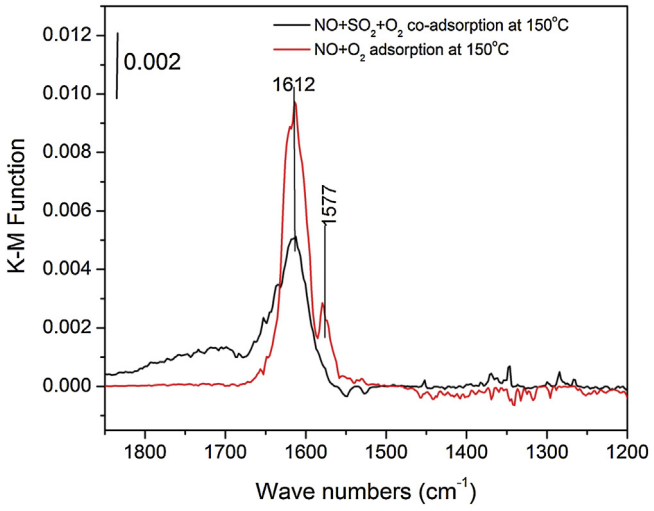

Fig. 8. DRIFTS spectra taken after a 60 min exposure to NO + O_2, and both SO_2 and NO + O_2 at 150 °C. Experimental conditions: 500 ppm NO, 10% O_2, 200 ppm SO_2 (if added) in a balance of He.

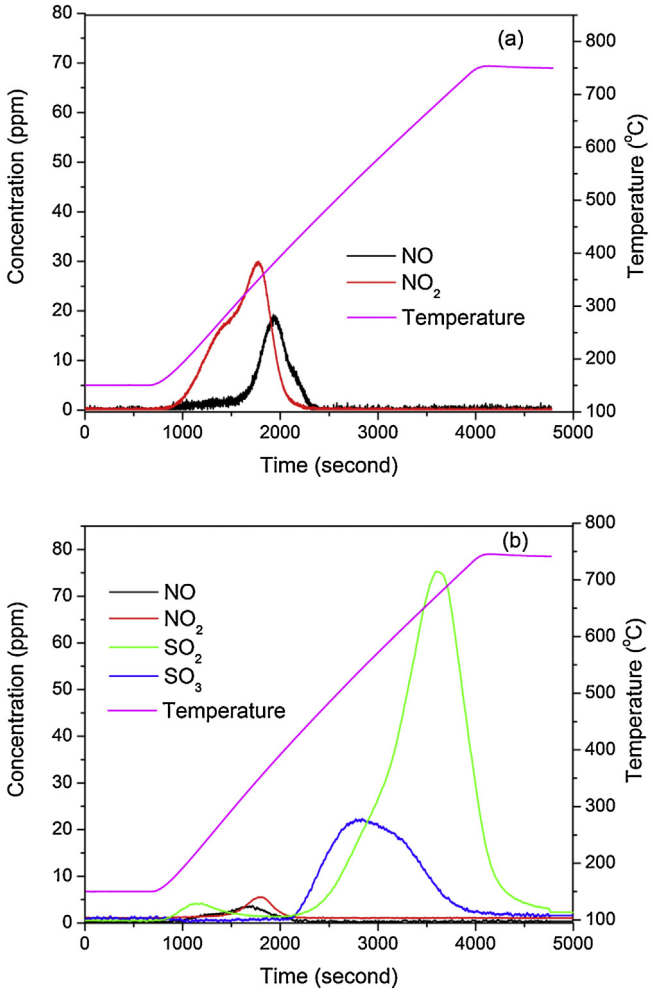

Fig. 9. TPD after exposure to (a) NO + O_2 and (b) SO_2 + NO + O_2. Experimental conditions: 500 ppm NO, 10% O_2, 200 ppm SO_2 (if added) in a balance of N_2 at 150 °C, purged by N_2, followed by the TPD with a heating rate of 10 °C/min in N_2.

3.9. TPD of adsorbed NO_x and adsorbed NO_x + SO_2

In order to further confirm the competitive adsorption of NO_x and SO_2, two TPD experiments were conducted for comparison. Fig. 9(a) shows the concentrations during a TPD after the catalyst was exposed to NO + O_2. A significant amount of NO (12.7 μmol/g) and NO_2 (31.1 μmol/g) desorbed from the catalyst surface. NO_2 was the primary species desorbed at temperatures below 375 °C, and at higher temperature, NO, with equilibrium limitations between NO and NO_2 playing a role. With SO_2 added during NO + O_2 adsorption, much less NO and NO_2 were released from the surface during the TPD experiment as compared to that in the absence of SO_2 during adsorption. In addition, some SO_3 (41.6 μmol/g) desorption was observed at temperatures above 400 °C and a large amount of SO_2 (126 μmol/g) desorbed at higher temperatures. These results further confirm SO_2 decreases NO_x adsorption extent. It is also worth mentioning that no SO_3 was detected during the TPD taken after SO_2 adsorption over the Cu-SAPO-34 catalyst (Fig. 5), while some SO_3 was formed on the catalyst during the co-adsorption process of both NO_x and SO_2. It has been reported that NO_2 can oxidize SO_2 to form SO_3 [32]. Therefore, it is likely that desorbing SO_2 was oxidized by NO_2 into SO_3, which was released at a relatively high temperature.

Based on the TPD and DRIFTS characterization data, exposure to SO_2 results in sulfate formation, which in turn leads to two possible degradation modes. First, there is clear evidence of $(NH_4)_2SO_4$ formation. Such species can foul surface sites, block pores and in general limit reactant/catalyst interactions. Second, exposure to SO_2 preferentially blocked key NO_x adsorption sites on the surface. Specifically, the formation of bidentate nitrate species, previously identified as the signature of NO_x stored on Cu sites, was considerably inhibited in the presence of SO_2. Of particular note, catalyst performance was only inhibited below 300 °C. Based on the TPD results, it is in this temperature range that the $(NH_4)_2SO_4$ decomposes. This therefore suggests that the formation of the $(NH_4)_2SO_4$ is the key low temperature SO_2 poisoning degradation mode.

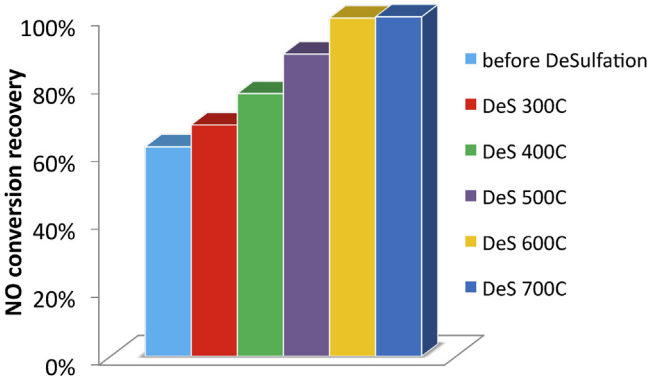

Fig. 10. NH_3-SCR activity after stepwise desulfation at different temperatures. Experimental conditions: 100 ppm SO_2, 500 ppm O_2 and a balance of N_2 at 130 °C for 3 h, purged by N_2, then pretreated at 300, 400, 500, 600 and 700 °C in 10% O_2/N_2, respectively. For every temperature, the pretreatment time was 12 h, then NH_3-SCR activity was evaluated at 260 °C.

3.10. Regeneration of the SO_2 poisoned catalyst by O_2/N_2

After SO_2 exposure, the Cu/SAPO-34 sample was heated to different temperatures (300–700 °C) in order to investigate the potential for SCR reaction activity recovery. Fig. 10 shows the NO conversion at 260 °C before and after the high temperature treatments. NO conversion in the presence of 50 ppm SO_2 reached only 61% of the original activity obtained in the absence of SO_2. However, if the catalyst was heated at 300 °C for 12 h after the SO_2 exposure, the catalyst activity attained 68% of the original SCR

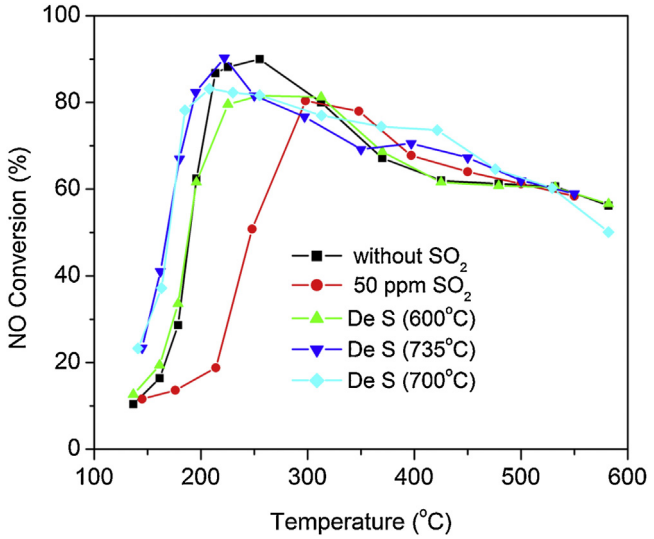

Fig. 11. NH_3-SCR activity with and without SO_2 and after a high temperature desulfation/regeneration exposure. Reaction conditions: 500 ppm NH_3, 500 ppm NO, 50 ppm SO_2, 10% O_2 in a balance of N_2. High temperature treatment at 600, 700, or 735 °C, respectively in 10% O_2/N_2 overnight.

performance. Furthermore, when the regeneration temperature was increased to 500 °C, at which temperature the $(NH_4)_2SO_4$ surface species were completely removed, 90% of the SCR performance was recovered, which strongly suggests that the SO_2 poisoning effect was mainly due to the formation of $(NH_4)_2SO_4$. Interestingly, there is still 10% NO conversion loss even if the $(NH_4)_2SO_4$ was removed from the catalyst surface. This is due to the formation of small amounts of $CuSO_4$ or $Ce_x(SO_4)_y$ on the catalyst. As previously discussed, these species typically decompose at a relatively high temperature. As shown in Fig. 11, indeed, with increasing the temperature above 500 °C, the NO conversion was further recovered. Almost 100% regeneration was achieved. Surprisingly, with the highest temperature exposure, higher low temperature activity was obtained relative to the fresh sample, which has been previously observed [23] and is likely due to further ion-exchange during the high temperature exposure.

4. Conclusions

In this study, the effect of SO_2 poisoning on the SCR reaction activity of a Cu-SAPO-34 catalyst was characterized. SO_2 did inhibit the reaction, specifically in the low temperature region (<300 °C). The SO_2 poisoning mechanism involves the formation of $(NH_4)_2SO_4$ species that may poison the active sites and block the zeolite pores. SO_2 adsorption also competes with NO_x adsorption on the Cu sites, also potentially contributing to the inhibition observed. SO_2 poisoning was reversible with NO conversions recovered after high temperature treatment in an O_2/N_2 mixture.

Acknowledgements

The authors gratefully acknowledge Cummins Inc for financial support.

Appendix A. Supplementary data

Supplementary data associated with this article can be found, in the online version, at http://dx.doi.org/10.1016/j.apcatb.2014.03.030.

References

[1] M. Iwamoto, H. Furukawa, Y. Mine, F. Uemura, S.-i. Mikuriya, S. Kagawa, Chem. Commun. 0 (1986) 1272–1273.
[2] R.G. Silver, M.O. Stefanick, B.I. Todd, Catal. Today 136 (2008) 28–33.
[3] Y. Cheng, C. Montreuil, G. Cavataio, C. Lambert, SAE Int. 01 (2009) 0898.
[4] P. Ballea, B. Geigera, D. Klukowskia, M. Pignatellia, S. Wohnraua, M. Menzelb, I. Zirkwac, G. Brunklausd, S. Kureti, Appl. Catal. B: Environ. 91 (2009) 587–595.
[5] V. Bacher, C. Perbandt, M. Schwefer, R. Siefert, T. Turek, Appl. Catal. B: Environ. 134–135 (2013) 55–59.
[6] L. Xu, R.W. McCabe, R.H. Hammerle, Appl. Catal. B: Environ. 39 (2002) 51–63.
[7] G. Qi, R.T. Yang, Appl. Catal. B: Environ. 60 (2005) 13–22.
[8] M. Høj, M. Josef Beier, J. Grunwaldt, S. Dahl, Appl. Catal. B: Environ. 93 (2009) 166–176.
[9] A. Sultana, T. Nanba, M. Sasaki, M. Haneda, K. Suzuki, H. Hamada, Catal. Today 164 (2011) 495–499.
[10] P.J. Andersen, H.Y. Chen, J.M. Fedeyko, E. Weigert, US Patents US20100267548 A1,10,21, 2010.
[11] D. Wang, L. Zhang, K. Kamasamudram, W.S. Epling, ACS Catal. 3 (2013) 871–881.
[12] W. Xu, H. He, Y. Yu, J. Phys. Chem. C 113 (2009) 4426–4432.
[13] J. Wang, T. Yu, X. Wang, G. Qi, J. Xue, M. Shen, W. Li, Appl. Catal. B: Environ. 127 (2012) 137–147.
[14] L. Ma, Y. Cheng, G. Cavataio, R.W. McCabe, L. Fu, J. Li, J. Chem. Eng. 225 (2013) 323–330.
[15] J.H. Kwak, D. Tran, S.D. Burton, J. Szanyi, J.H. Lee, C.H.F. Peden, J. Catal. 287 (2012) 203–209.
[16] J.H. Kwak, R.G. Tonkyn, D.H. Kim, J. Szanyi, C.H.F. Peden, J. Catal. 275 (2010) 187–190.
[17] P.J. Andersen, H.Y. Chen, J.M. Fedeyko, E. Weigert, US Patents EP2698192 A1,02,19, 2014.
[18] Y. Cheng, C. Lambert, D.H. Kim, J.H. Kwak, S.J. Cho, C.H.F. Peden, Catal. Today 151 (2010) 266–270.
[19] B. Ramachandran, R.G. Herman, S. Choi, H.G. Stenger, C.E. Lyman, J.W. Sale, Catal. Today 55 (2000) 281–290.
[20] B.Q. Jiang, Z.B. Wu, Y. Liu, S.C. Lee, W.K. Ho, J. Phys. Chem. C 114 (2010) 4961–4965.
[21] S. Yang, Y. Guo, H. Chang, L. Ma, Y. Peng, Z. Qu, N. Yan, C. Wang, J. Li, Appl. Catal. B: Environ. 136 (2013) 19–28.
[22] M. Ziolek, I. Sobczak, I. Nowak, M. Daturi, J.C. Lavalley, Top. Catal. 11 (2000) 343–350.
[23] L. Wang, J.R. Gaudet, W. Li, D. Weng, J. Catal. 306 (2013) 68–77.
[24] G. Li, S.C. Larsen, V.H. Grassia, J. Mol. Catal. A: Chem. 227 (2005) 25–35.
[25] I.C. Marcu, I. Sandulescu, J. Serbian Chem. Soc. 69 (2004) 563–569.
[26] H. Abdulhamid, E. Fridell, J. Dawody, M. Skoglundh, J. Catal. 241 (2006) 200–210.
[27] C.C. Chang, J. Catal. 53 (1978) 374–385.
[28] F. Yin, A.L. Blumenfeld, V. Gruver, J.J. Fripiat, J. Phys. Chem. B 101 (1997) 1824–1830.
[29] D. Klukowski, P. Balle, B. Geiger, S. Wagloehner, S. Kureti, B. Kimmerle, A. Baiker, J.D. Grunwaldt, Appl. Catal. B: Environ. 93 (2009) 185–193.
[30] H. Chang, J. Li, J. Yuan, L. Chen, Y. Dai, H. Arandiyan, J. Xu, J. Hao, Catal. Today 201 (2013) 139–144.
[31] G.Y. Xie, Z.Y. Liu, Z.P. Zhu, Q.Y. Liu, J. Ge, Z.G. Huang, J. Catal. 224 (2004) 36–41.
[32] G. Chen, J. Gao, J. Gao, Q. Du, X. Fu, Y. Yin, Y. Qin, Ind. Eng. Chem. Res. 49 (2010) 12140–12147.
[33] L. Zhang, J. Pierce, V.L. Leung, D. Wang, W.S. Epling, J. Phys. Chem. C 117 (2013) 8282–8289.